Modeling the dynamics of the rotation-vibration generator for a flow-fruit detacher

Dechko Ruschev[1], Stoyan Ishpekov[2*], Petar Petrov[2]

(1. *Technical University - Sofia, Plovdiv Branch, Department of Mechanics, Plovdiv 4000, Bulgaria*;

2. *Agricultural University, Department of Agricultural Mechanization, Plovdiv 4000, Bulgaria*)

Abstract: The investigation aimed at modeling the dynamics of the rotational-vibration generator, which is widely used for driving fruit detachers at harvesting of many crops like grape, tomatoes, blueberries, raspberries, chokeberry, black currant, sesame seeds etc. The research of the obtained model was performed by software written in FORTRAN and by using the LabView environment as input-output interface. The model has a relative error for the carrier angular amplitude of 0.48% compared to the one, determined by an experimental fruit detacher. The effect of vibration generator parameters on its dynamic characteristics was also defined. It was found out that the angular amplitude of the vibration generator is unstable parameter, which is a prerequisite for quality indices reduction of the existing fruit detachers. This demands its construction modification in order to provide independent regulation of vibration amplitude and frequency, as well as for setting the ratio of angular amplitudes in both directions of carrier rotation. The obtained results can be used for the design and the adjustment of rotation-vibration generator for flow-fruit detachers.

Keywords: flow-fruit detacher, rotation-vibration generator, modeling

1 Introduction

To detach fruits of berry and vegetable crops as well as some seeds from twigs or stems, three major type mechanisms - slapper, sway and vibratory are used (Peterson and Brown, 1996; Ishpekov et al., 2016; Ishpekov et al., 2017). The fruit detacher of vibratory type is most frequently used in the present harvesters (Takeda et al., 2008). The vibrations are created by a rotation - vibratory generator (RVG) which drives the device for detaching fruits from twigs and stems. It generates angular vibrations with frequency reaching 12 Hz by two eccentric weights turning in opposite directions. The vibrations are transmitted to spindles or discs with metal or plastic rods. They also rotate with an average peripheral speed, close to the harvester speed, as result of rods penetration among the twigs and their reaction. The force for rotating the spindles is significant, because RVG creates only angular vibrations with equal amplitudes in both directions (Yu et al., 2014), therefore the crops are tilted in the direction of forward speed of the harvester. This is the main reason for low operational speed and low capacity of harvesters as well as for mechanical damaging of crops and their fruits (Rabcewicz et al., 2010; Caprara et al., 2014). The impact of existing fruit detachers causes damage of berry fruits and subsequent leakage of juice. Its quantity in the product harvested by machine reaches up to 25%-30% of the total mass. This causes several negative effects such as oxidation of phenolics, abnormal fermentation, etc. (Pezzi et al., 2013).

The target of the current study is to model the dynamics of the rotational-vibration generator with respect to determine the reasons for its functional disadvantages as a driving mechanism of flow fruit detachers.

2   Methodology

A dynamic model of the RVG through Lagrange equation was drawn. The kinetic energy of the generator was expressed and used to obtain the differential equation of motion. The second order Lagrange equation was used for solving the differential equations for motion of the mechanical system. The relation between angular velocities and angles of rotation was obtained by the method of Willis (Willis, 1870). Generalized forces were determined by the expression for virtual work of external and internal forces and momentums. The resulting equation was solved by using dimensionless variables with the aim to reduce the number of parameters. Differential equations were solved numerically by the method of Runge-Kutta of eighth order with variable step and usage the algorithm of Dorman and Prince (Dormand and Prince, 1978). The algorithm was implemented as a subroutine of FORTRAN language in a virtual instrument developed in the environment of software LabView (www.ni.com/labview). It was also used for conducting the numerical experiments as well as for the identification of model unknown parameters. The identification was made through the comparison the angular amplitude of RVG carrier of both numerical results from the virtual instrument and measured output data from an experimental fruit detacher (Ishpekov et al., 2015). Experiments were implemented according to a symmetrical compositional plan B_3 (Mitkov et al., 1993). The experimental data were processed by least squares regression analysis by made of use STATISTICA software (www.statsoft.com). The model error was estimated by comparing the angular amplitude of the carrier, obtained by numerical experiment and by physical experiment conducted with the experimental fruit detacher, which was driven by RVG. The resulting model was investigated numerically in both cases - with and without resistance and load on the RVG carrier.

3   Results

3.1   RVG description

RVG resembles the inertial transformer of torque with Chalmers pulse mechanism (Lester, 2009). In both constructions, unbalanced planetary wheels generate the vibrations. RVG carrier turns rod spindle, which gives vibrations to plants for detachment their fruits. The principle scheme of RVG is shown in Figure 1. It consists of two sets of details:

- Fly-wheel, which is connected to the sun gear 1, rotating at a constant angular speed ω_0,

- Loading unit, consisting of planet gears 2 to which are attached eccentrically located weights and carrier 3, playing the role of a reactor.
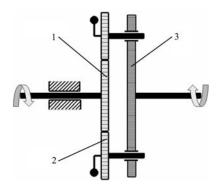

Figure 1   Scheme of rotational vibration generator

The considered RVG has two degrees of freedom which are used to determine the position of mechanism and two independent parameters are required. The first one is the angle of rotation of the carrier and the second one is the angle of rotation of the central wheel. Inherently, it is a differential mechanism with one sun gear. In the laboratory, this mechanism is driven by a frequency-controlled ac motor, which maintains constant angular velocity. For this reason, the assumption has been made that the drive has unlimited power and sun gear rotates at a constant angular velocity.

3.2   Development of dynamic model

The kinematic scheme of RVG is shown in Figure 2. It has been assumed that central gear, planet gear and carrier rotate in the same direction with angular speeds ω_0, ω_2 and ω_1 respectively.
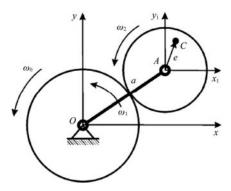

Figure 2   Kinematic scheme of RVG

The used Lagrange Equation (1) is

$$\frac{d}{dt}\left(\frac{\partial E_k}{\partial \dot{q}_i}\right) - \frac{\partial E_k}{\partial q_i} = Q_i, \quad i = 1, 2 \qquad (1)$$

where, E_k is the kinetic energy of the system; Q_1 and Q_2 are generalized forces.

The rotation angle of the central wheel φ_0 and the rotation angle of the carrier φ_1 are adopted as generalized coordinates.

3.3 Kinetic energy of the system

It is the sum of kinetic energies of the central gear and all rigidly connected parts:

$$E_k = \frac{1}{2}J_0\omega_0^2 + \frac{1}{2}J_1\omega_1^2 + \frac{1}{2}m_2v_A^2 + \frac{1}{2}J_2\omega_2^2 + m_2\vec{v}_A \cdot \vec{v}_{C_r} \quad (2)$$

where, E_{k0} is the kinetic energy of planet gears; E_{k2} is the kinetic energy of attached eccentrically located loads; E_{k1} is the kinetic energy of carrier and attached unit; J_0, J_1, J_2 are the inertia momentums toward axes of central gear, carrier and planet gears; m_2 is the mass of planet gears; v_A is the rotation speed of the axis of planet gear; v_{C_r} is the relative velocity of planet gear gravity centre.

$$\vec{v}_A = [-\omega_1 y_A, \omega_1 x_A, 0]^T, \quad \vec{v}_{C_r} = [-\omega_2 y_{1C}, \omega_2 x_{1C}, 0]^T,$$

$$\vec{v}_A \cdot \vec{v}_{C_r} = \omega_1\omega_2(y_A y_{1C} + x_A x_{1C}) \qquad (3)$$

$$x_A = a\cos\varphi_1, \quad y_A = a\sin\varphi_1, \quad x_{1C} = e\cos\varphi_2,$$

$$y_{1C} = e\sin\varphi_2, \quad v_A = \omega_1 a \qquad (4)$$

$$\vec{v}_A \cdot \vec{v}_{C_r} = \omega_1\omega_2 a\, e\cos(\varphi_2 - \varphi_1) \qquad (5)$$

Applying the method of Willis for the relation between angular velocities and angles of rotation give us the following relations:

$$\frac{\omega_2 - \omega_1}{\omega_0 - \omega_1} = -i \qquad (6)$$

$$\omega_2 = (i+1)\omega_1 - i\omega_0, \quad \varphi_2 - \varphi_1 = i(\varphi_1 - \varphi_0) \qquad (7)$$

where, i is the gear ratio of engagement.

After substituting of Equation (2) to (7), for the kinetic energy of mechanical system is obtained:

$$E_k = \frac{1}{2}(J_0 + i^2 J_2)\omega_0^2 + \frac{1}{2}(J_1 + (i+1)^2 J_2 + m_2(a^2 +$$
$$2(i+1)a\,e\cos(i(\varphi_1 - \varphi_0))))\omega_1^2 - \qquad (8)$$
$$\left(i(i+1)J_2 + im_2 a\,e\cos(i(\varphi_1 - \varphi_0))\right)\omega_0\omega_1$$

3.4 Generalized forces

At working the following momentums act on RVG:

- Driving momentum M_0, which is determined by the

stability of central gear angular velocity;

- Momentum of the load M_L, acting on the shaft of carrier. It has been assumed that this momentum has three components. The first M_C has constant size and gives an account for dry friction in the carrier suspension and between carrier and stems. The second M_L and third M_{12} components depend on first and second degree of the angular velocity of carrier respectively with the coefficients of proportionality μ'_1 and μ''_1 accordingly.

$$M_L = -M_C\,\text{sgn}(\omega_1) - \mu'_1\omega_1 - \mu''_1\omega_1^2\,\text{sgn}(\omega_1) \qquad (9)$$

- Momentum of resistance, acting between planet gear and carrier M_{12}. It has been assumed that it depends on first and second degree of the relative angular velocity with coefficients μ'_{12} and μ''_{12}.

$$M_{12} = -\mu'_{12}(\omega_2 - \omega_1) - \mu''_{12}(\omega_2 - \omega_1)^2\,\text{sgn}(\omega_2 - \omega_1) \quad (10)$$

For generalized forces Q_0 and Q_1 we can write

$$\delta A = M_0\delta\varphi_0 + M_L\delta\varphi_1 - M_{12}(\delta\varphi_2 - \delta\varphi_1) = Q_0\delta\varphi_0 + Q_1\delta\varphi_1 \qquad (11)$$

The relative angular velocity of planet gear $\omega_2 - \omega_1$ and the virtual relative rotation angle $\delta\varphi_2 - \delta\varphi_1$ according to Equation (6) and (7) are:

$$\omega_2 - \omega_1 = i(\omega_1 - \omega_0), \quad \delta\varphi_2 - \delta\varphi_1 = i(\delta\varphi_1 - \delta\varphi_0) \quad (12)$$

After substitution of Equation 9 to 11 for generalized forces are obtained the following expressions:

$$Q_0 = M_0 + i^2\mu'_{12}(\omega_1 - \omega_0) + i^3\mu''_{12}(\omega_1 - \omega_0)^2\,\text{sgn}(\omega_1 - \omega_0)\mu''_{12}$$
$$Q_1 = -M_C\,\text{sgn}(\omega_1) - \omega_1\mu'_1 - \omega_1^2\,\text{sgn}(\omega_1)\mu''_1 - i^2(\omega_1 - \omega_0)$$
$$\mu'_{12} - i^3(\omega_0 - \omega_1)^2\,\text{sgn}(\omega_1 - \omega_0)\mu''_{12}$$

$$(13)$$

3.5 Differential equations of motion

The expression for kinetic energy is differentiated by generalized coordinates and speeds, as well as by time. The results obtained are substituted in Equation (1) together with expressions for generalized forces (Equation (13)). The following system of differential equations is obtained:

$$(J_0 + i^2 J_2)\ddot{\varphi}_0 - i\left((1+i)J_2 + aem_2\cos(i(\psi_0 - \psi_1))\right)\ddot{\varphi}_1 +$$
$$iaem_2\omega_1^2\sin(i(\varphi_0 - \varphi_1)) = Q_0 - ((1+i)J_2 +$$
$$aeim_2\cos(i(\varphi_0 - \varphi_1)))\ddot{\varphi}_0 + (J_1 + (1+i)^2 J_2 +$$
$$a^2 m_2 + 2ae(1+i)m_2\cos(i(\varphi_0 - \varphi_1)))\ddot{\varphi}_1 +$$
$$aem_2(i(i(\omega_0 - \omega_1)^2 + \omega_1(\omega_1 - 2\omega_0))\sin(i(\varphi_0 - \varphi_1))) = Q_1$$

$$(14)$$

The RVG is driven by an engine with a frequency controller Schneider Electric - ATV12HU22M2 (www.mouser.bg) which maintains a constant angular velocity of the central gear. For this reason, $\ddot{\varphi}_0 = 0$, $\omega_0 = const$, $\varphi_0 = \omega_0 t$. Under these conditions, the differential equations system is solved on $\ddot{\varphi}_1$.

$$\ddot{\varphi}_1 = \frac{Q_1 - aem_2 i(i(\omega_0 - \omega_1)^2 + \omega_1(\omega_1 - 2\omega_0))\sin(i(\omega_0 t - \varphi_1))}{J_1 + (1+i)^2 J_2 + a^2 m_2 + 2aem_2(1+i)\cos(i(\omega_0 t - \varphi_1))}$$

$$t = 0, \quad \varphi_1 = 0, \quad \dot{\varphi}_1 = 0$$

$$(15)$$

Obviously, the right side of resulting expression includes only the generalized force Q_1. Therefore, the expression of M_0 is not defined and is not used.

3.6   Transition to dimensionless variables

The resulting Equation (15) depends on fifteen constructive parameters (Figure 4). The introduction of dimensionless variables reduces the number of parameters to seven and received results are more compendious. A dimensionless time is entered $\tau = t\omega_0$. Derivatives in dimensionless time are indicated in the following way:

$$\frac{d\varphi_1}{d\tau} = \varphi_1' = \tilde{\omega}_1 \qquad (16)$$

$$\frac{d^2\varphi_1}{d\tau^2} = \frac{d\tilde{\omega}_1}{d\tau} = \tilde{\omega}_1' = \varphi_1'' \qquad (17)$$

After conversion to dimensionless variables is obtained the following equation:

$$\varphi_1'' = \frac{\tilde{Q}_1 - i(i(1-\varphi_1')^2 + \varphi_1'(\varphi_1'-2))\sin(i(\tau-\varphi_1))}{\tilde{J} + 2(1+i)\cos(i(\tau-\varphi_1))} \qquad (18)$$

$$\tau = 0, \quad \varphi_1 = 0, \quad \varphi_1' = 0$$

where, $\tilde{Q}_1 = \dfrac{Q_1}{aem_2\omega_0^2}$ is the dimensionless generalized

force; $\tilde{J} = \dfrac{J_1 + (1+i)^2 J_2 + a^2 m_2}{aem_2}$ is the dimensionless

momentum of inertia.

If the expression for dimensionless generalized force is substituted in Equation (13) then is obtained:

$$\tilde{Q}_1 = -\tilde{M}_C \,\text{sgn}(\tilde{\omega}_1) - \tilde{\mu}_1' \tilde{\omega}_1 - \tilde{\mu}_1'' \tilde{\omega}_1^2 \,\text{sgn}(\tilde{\omega}_1) - \qquad (19)$$
$$\tilde{\mu}_{12}'(\tilde{\omega}_1 - 1) - \tilde{\mu}_{12}''(1 - \tilde{\omega}_1)^2 \,\text{sgn}(\tilde{\omega}_1 - 1)$$

where,

$$\tilde{M}_C = \frac{M_C}{aem_2}\frac{1}{\omega_0^2}, \quad \tilde{\mu}_1' = \frac{\mu_1'}{aem_2}\frac{1}{\omega_0}, \quad \tilde{\mu}_1'' = \frac{\mu_1''}{aem_2},$$

$$\tilde{\mu}_{12}' = \frac{i_{12}^2 \mu_{12}'}{aem_2}\frac{1}{\omega_0}, \quad \tilde{\mu}_{12}'' = \frac{i_{12}^3 \mu_{12}''}{aem_2} \qquad (20)$$

The analysis of Equation (19) and (20) about the impact of angular velocity on generalized force and hence on the solution of Equation (18) shows the results as follows:

- Dimensionless variables depend on constructive parameters a, e, m_2, i, i_{12}, J_1 и J_2. They remain constant when changing the RVG mode for the reason that they do not depend on the angular velocity ω_0. The influence of momentum M_C is reduced proportionately to the second degree of angular velocity ω_0. Therefore, at high engine speed, the dry friction has only a negligible impact on the dynamics of RVG and on the amplitude of angular oscillations.

- The factors depending on the first degree of angular velocity of carrier (μ_1', μ_{12}''), reduce in proportion to the first degree of rotational speed of the engine. This shows that their influence on dynamics is less at high speed.

- Factors depending on second degree of angular velocity of the carrier (μ_1', μ_{12}''), do not depend on rotational speed of the drive. It follows that their impact on the dynamics is not changed with the increasing engine speed. The amplitude of angular oscillations of carrier remains constant if the addends depending on the first degree of angular velocity and the permanent member is ignored.

3.7   Numerical solution

The resulting differential equation has no analytical solution. Therefore, a numerical solution is found out by the method of Runge - Kutta with a local accuracy $\varepsilon = 1.0 \ 10^{-14}$ (Hairer et al., 2009). According to the theorems of existence and uniqueness for the first order ODE's, the right side of Equation 18 must be a continuous function. Besides that, it must have continuous partial derivatives with respect to the unknown function ω_1 in the range, where solution is sought. From Equation (9), it is clear that for the momentum M_L, these conditions are not met. This requires a change of this expression with such, for which exists solution of the differential equation. It is approximated by a continuous and differentiable function, which consists of two parts:

$$\tilde{M}_L = -\text{sgn}(\tilde{\omega}_1) \begin{cases} a_0 + a_1|\tilde{\omega}_1| + a_2^2\tilde{\omega}_1^2 & ; \; |\tilde{\omega}_1| < \delta \\ \tilde{M}_C + \tilde{\mu}_1'|\tilde{\omega}_1| + \tilde{\mu}_1''\tilde{\omega}_1^2 & ; \; |\tilde{\omega}_1| \geq \delta \end{cases} \quad (21)$$

where, δ is a small number. In this study $\delta=0.001s^{-1}$.

In order to establish the reliability of this assumption, numerical experiments with different values of δ are made. It is established that at $\delta<0.01$ its value does not affect on the angular velocity and the amplitude of oscillation.

Coefficients a_0, a_1 and a_2 are determined by conditions of smoothness and continuity of function in the points $\tilde{\omega}_1 = 0$ and $|\tilde{\omega}_1| = \delta$.

$$a_0 = 0, \; a_1 = \tilde{\mu}_1' + \frac{2\tilde{M}_C}{\delta}, \; a_2 = -\frac{\tilde{M}_C}{\delta^2} + \tilde{\mu}_1'' \quad (22)$$

In Figure 3 the function in the range $\tilde{\omega}_1 \in (-0.005, 0.005)$ is shown. It is continuous and differentiable at the point $\delta=0.001s^{-1}$.
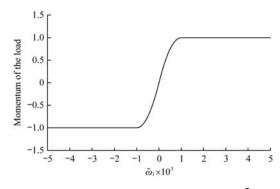

Figure 3   Approximation of expression for $\tilde{M}_L$

4   Numerical experiment

Results of numerical modeling in fact are the laws for carrier angle rotation and its angular speed depending on time, obtained in form of numerical ranks. The most important results are both obtained amplitude of rotation angle and average angular velocity of the carrier. They predetermine the main qualitative and quantitative indicators of the flow-fruit detacher driven by RVG. The variations of both indicators are investigated through numerical experiments, depending on model parameters and coefficients of resistantg momentums, which vary in range important for practice.

The investigation uses the dimensionless form of differential Equation (19) and (20). It has only one parameter - the dimensionless momentum of inertia, which effects on dynamics of RVG when working without resistance. The numerical experiments are carried out through a virtual instrument, which allows to determine all parameters of RVG after entering its mechanical parameters and integration conditions (Figure 4).

4.1   Motion without resistance

The laboratory experiment is made without load from stems and for this reason the friction momentums in the connecting links are small and can be neglected. The numerical experiments to study the model of RVG are made through the dimensionless parameter, which values vary in the limits $3.01 \leq \tilde{J} \leq 100$, $i=1$ (Figure 5). It is evident that there are two asymptotes, which constrain the variation of dimensionless momentum of inertia and the carrier amplitude. By increasing the dimensionless momentum of inertia, the amplitude tends to 0.01 and the RVG loses its functionality. Reducing the dimensionless parameter to 3.0, the angular amplitude goes to infinity. Values of $\tilde{J}$ with practical application lie in the range 5 to 15. The developed experimental fruit detacher has $\tilde{J} = 9.46667$.

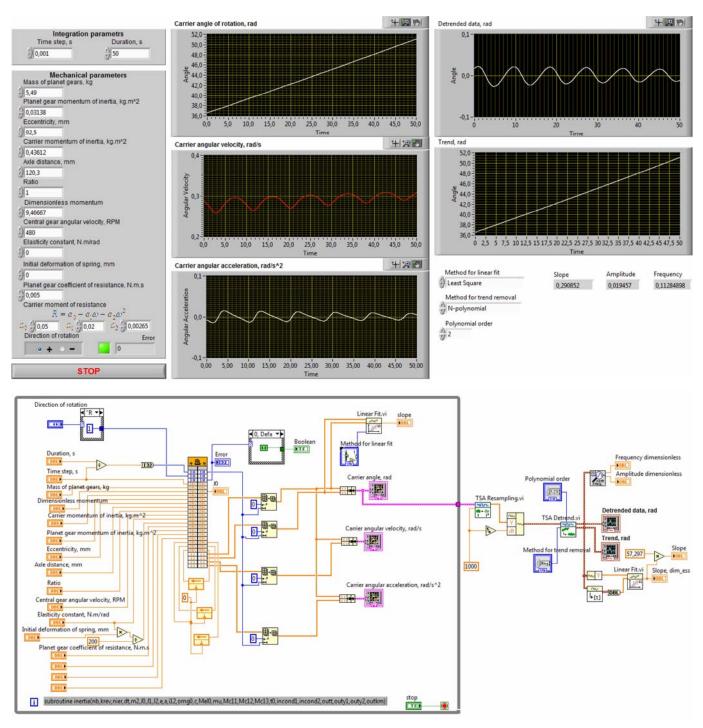The average angular velocity of carrier is zero at all values of $\tilde{J}$ and the period of oscillation is 2π. This is according to Equation (18), which right side at $\tilde{Q}_1 = 0$ is a periodic function with a period 2π and with settled oscillations. The solution is a periodic function with the same period. In Figure 6, the law of carrier motion without resistance and $\tilde{J} = 9.46667$ with aim to assess the working reliability of experimental RVG is shown.
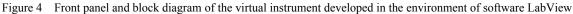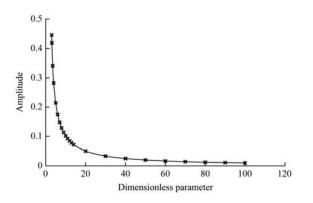
4.2   Motion with resistance

The dependence of resistance coefficients on average angular velocity, amplitude and vibration frequency of the carrier is determined in this section. All studies are made at the value of dimensionless momentum $\tilde{J} = 9.46667$, which has been obtained for the experimental fruit detacher (Ishpekov et al., 2015).
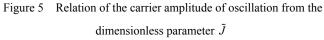
4.2.1   Impact of momentum $\tilde{M}_C$

In the Figure 7, the change of amplitude and average angular velocity of the carrier, depending on momentum $\tilde{M}_C$ (Equation (19) and (20)) is shown and illustrates the impact of dry friction in RVG.

Figure 4   Front panel and block diagram of the virtual instrument developed in the environment of software LabView

Figure 5   Relation of the carrier amplitude of oscillation from the dimensionless parameter $\tilde{J}$
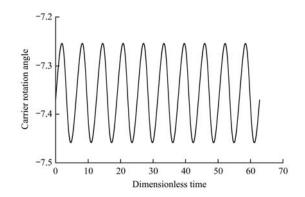
Figure 6   Graph of the carrier motion law digitally obtained through the virtual instrument
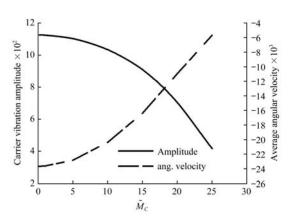
Figure 7   Variation of the average amplitude and angular velocity of the carrier depending on momentum $\tilde{M}_C$

The effect of dry friction occurs mainly in interaction of the working body with stems. It is absent or extremely small in laboratory conditions. Measurements taken at the Agricultural University - Plovdiv show that the momentum of dry friction does not exceed 10 N·m. Real operating conditions occur at sun gear frequency in the range 8 to 12 Hz. According to Equation (19) and (20), the dimensionless momentum $\tilde{M}_C$ does not exceed 2, when a=120 mm and e=92 mm (Figure 2).

The main results of numerical analysis for influence of dry friction momentum are:

- Momentum $\tilde{M}_C$ virtually has no effect on the angular amplitude of carrier;

- Dry friction momentum causes rotation of the carrier with a small average angular velocity in direction opposite to rotation of central wheel. It decreases with the increasing of dry friction momentum and is caused by the asymmetry of angular velocity. As shown in Figure 8, the period of carrier in positive direction of rotation is greater than the one in negative direction. This is due to the constant dry friction momentum and to negative direction of the average momentum, acting on carrier.
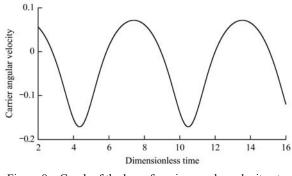

Figure 8   Graph of the law of carrier angular velocity at a resistance momentum value of $\tilde{M}_C = 5$

4.2.2   Impact of coefficients $\tilde{\mu}_1'$ and $\tilde{\mu}_1''$

As shown in Figure 9, the carrier amplitude depends on coefficients $\tilde{\mu}_1'$ and $\tilde{\mu}_1''$ (6) at an angular velocity of the sun gear ω_0=1.0Hz. The numerical experiments indicate that average angular velocity of carrier is also equal to zero at $\tilde{\mu}_1'' = 0$ irrespective of coefficient $\tilde{\mu}_1'$ value. When changing the coefficient $\tilde{\mu}_1''$ in the range 0.5 to 100, the carrier average angular velocity changes from 0.0078 to 0.0052, which indicates weak relation.

This indicates that coefficient $\tilde{\mu}_1''$ which depends on second degree of the angular velocity of carrier (ω_1^1) has lower impact on carrier amplitude than the coefficient $\tilde{\mu}_1'$, which depends on ω_1.
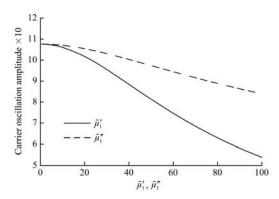

Figure 9   Carrier oscillation amplitude depending on coefficients of proportionality $\tilde{\mu}_1'$ and $\tilde{\mu}_1''$

4.2.3   Impact of coefficients $\tilde{\mu}_{12}'$ and $\tilde{\mu}_{12}''$

The results about impact of viscous resistance between the planet and carrier show that after a short transitional period, it is established a stable motion if other coefficients of resistance are equal to 0. The carrier amplitude is equal to zero and its angular speed matched the angular velocity of sun gear (7).

5   Coefficients identification and model error

The operation of RVG depends on the resistance that planetary gears and carrier render. The resistance of planetary gears can be considered constant and proportional to the coefficient a_2. The reaction of carrier is on the form

$$R = a_0 + a_1 \cdot \omega + a_2 \cdot \omega^2 \tag{23}$$

where, a_0 is the resistance coefficient of dry friction in the connections of carrier; a_1 is the resistance coefficient of viscous friction; a_2 is the resistance coefficient of loading

with processed stems.

The coefficients depend on the specific construction of the fruit detacher and working conditions. The coefficient $a_2=0$ when stems are not delivered in the fruit detacher. The values of other coefficients are determined through identification which is conducted by comparing the results from numerical and laboratory experiments. The numerical experiment is performed by the virtual instrument (Figure 4). The laboratory experiment is conducted through a developed fruit detacher (Figure 10). Controllable factors are mentioned coefficients and the response is the relative error - e of model angular amplitude in comparison to the amplitude of fruit detacher.

The carrier angular amplitude is measured by an electronic system. It consists of an incremental encoder, data acquisition module USB-1208HS-2AO (www.mccdaq.com) and a computer (Figure 10). During the measurement, RVG rotates the encoder's rotor and its signal is read by the module and is delivered to the computer via USB. The signal is displayed through the virtual instrument after removing its trend. After that, the angular amplitude of carrier is determined.

Figure 10   Measuring the angular amplitude of RVG carrier which is part of an experimental fruit detacher

The following second order regression equation is received:

$$e = 255.231 - 3591.6778a_s + 4475.6327a_s^2 + 2617.111a_0 - 2276a_0^2 - 1662.5376a_1 + 4475.6327a_1^2$$

(24)

with determination coefficient $R^2=0.91$ and probability $p=0.052$.

Equal level lines obtained from regression Equation 24 are presented in Figure 11. It is seen that the error e has a minimum at $a_s=0.4$, $a_0=0.6$ and $a_1=0.4$. With these values of coefficients, the numerical model achieves
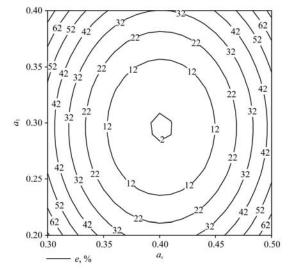
relative error $e=0.48\%$.

Figure 11   Contour plot of the relative error of numerical model depending on coefficients a_s and a_1, conditioned $a_0=0.6$

In Figure 12, the influence of coefficients a_s, a_0 and a_1 on the relative error of numerical model e are presented. It is evident that each coefficient varies with a small value of 0.2, but this leads to a significant growth of the model relative error from 30% to 70% as well as to a change of its sign. Practically, it means that:

- The error of numerical model is highly dependent on the precision of coefficients determination.

- The magnitude of carrier angular amplitude is highly dependent on factors that change during operation. This causes unstable operation of the fruit detacher driven by RVG and is a prerequisite for lowering its quality indices.
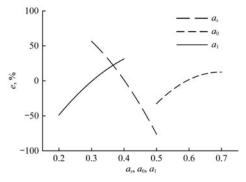

Figure 12   Dependence of relative error e on coefficients a_0, a_s and a_1

The received mathematical model of RVG and its numerical realization can be used for three practical tasks:

- Studying the influence of RVG parameters upon the magnitude of average angular velocity and oscillating amplitude of the fruit detacher.

- Designing of RVG which create oscillations of fruit

detachers for many different crops.

- Adjusting of RVG as part of a flow-fruit detacher according working conditions.

6   Conclusions

A dynamic model of a rotational-vibration generator (RVG) for a flow-fruit detacher has been developed and realized as a numeric model which relative error is 0.48%. It allows to conduct numeric investigation of the RVG indicators during its designing and before manufacturing. The results of investigations evidence that:

- The factors depending on the first degree of angular velocity of carrier reduce in proportion to the first degree of rotational speed of the sun gear. Thus, their influence on dynamics is less at high speed.

- Factors depending on second degree of angular velocity of the carrier do not depend on rotational speed of the sun gear. It follows that their impact on the dynamics is not changed with the increasing engine speed.

- By increasing the dimensionless momentum of inertia, the amplitude tends to 0.01 and the RVG loses its functionality. Reducing the dimensionless momentum of inertia to 3.0, the angular amplitude goes to infinity. Values of the dimensionless momentum of inertia with practical application lie in the range 5 to 15.

The amplitude of angular oscillation created by RVG depends slightly from resisting momentums and their coefficients. They are difficult to maintain constant or to change for adjusting working modes. This is a prerequisite for lowering the quality indicators of the harvester and flow-fruit detacher integrated.

The other parameter defining the performance of fruit detacher is the average angular velocity of carrier. The results indicate that its direction of rotation and its average are influenced by the coefficients of resisting momentums. For this reason, the use of RVG to implement sustainable operation of fruit detacher is not appropriate for each working condition.

To achieve sustainable operation of the flow-fruit detacher in changing fields' conditions and be adaptable when changing crop, it is not enough to rely only on resisting momentums and their coefficients. A constructional change of RVG is needed for changing its mechanical behavior.

References

Caprara, C., and F. Pezzi, 2014. Evaluation of quality of harvest and mechanical aspects related to beater adjustments in mechanical grape harvesting. *Transactions of the ASABE*, 57(4): 991–997.

Dormand, J. R., and P. J. Prince, 1978. New Runge-Kutta algorithms for numerical simulation in dynamical astronomy. *Celestial Mechanics*, 18223–232.

Hairer, E., S. P. Norsett, and G. Wanner. 2009. *Solving Ordinary Differential Equations I: Nonstiff Problems* (2nd rev. ed.), Heidelberg: Springer.

Ishpekov, S., P. Petrov, D. Ruschev, and R. Zaykov. 2015. Flow rotational fruit detacher with non-symmetric angular vibrations. Bulgarian Patent No. 3143.

Ishpekov, S., P. Petrov, R. Zaykov, and N. Naydenov. 2017. Indicators of a Fruit Detacher with non-symmetric angular oscillations at removing tomato fruits. *Research in Agricultural Engineering*, in press.

Ishpekov, S., R. Zaykov, and D. Ruschev, 2016. Indices of flow fruit detacher with angular vibrations at inertial threshing of sesame. *CIGR Journal,* 18(2): 94–102.

Lester, W. T. 2009. Continuously variable transmission using oscillating torque and one-way drives. United States Patent No. 7481127 B2.

Mitkov, A., and D. Minkov. 1993. *Statistical Methods for Investigation and Optimization of Agricultural Machinery*. Sofia: Zemizdat.

Peterson, D. L., and G. K. Brown. 1996. Mechanical harvester for fresh market quality blueberries. *Transactions of the ASAE,* 39: 823–827.

Pezzi, F., G. Balducci, and L. Pari. 2013. A new system to preserve quality of grapes harvested by machine. *Horticulture,* 978(13): 191–198.

Rabcewicz, J., and J. Danek. 2010. Evaluation of mechanical harvest quality of primo cane raspberries. *Journal of Fruit and Ornamental Plant Research*, 18(2): 239–248.

Takeda, F., G. Krewer, and E. L. Andrews, B. Mullinix, D. L. Peterson. 2008. Assessment of the V45 blueberry harvester on rabbit eye blueberry and southern high bush blueberry pruned to V-shaped canopy. *HortTechnology*, 18(1): 130–138.

Willis, R. 1870. *Principles of Mechanism*, 2nd ed. London: Longmans, Green co.

Yu, P., C. Li, F. Takeda, G. Krewer, G. Rains, and T. Hamrita. 2014. Measurement of mechanical impacts created by rotary, slapper and sway blueberry mechanical harvesters. *Computers and Electronics in Agriculture,* 101(4): 84–92.